

# Quantitative feedback controller design and test for an electro-hydraulic position control system in a large-scale reflecting telescope\*

Xiong-bin PENG<sup>†‡1,2</sup>, Guo-fang GONG<sup>1</sup>, Hua-yong YANG<sup>1</sup>, Hai-yang LOU<sup>1</sup>, Wei-qiang WU<sup>1</sup>, Tong LIU<sup>1</sup>

(<sup>1</sup>State Key Laboratory of Fluid Power Transmission and Control, Zhejiang University, Hangzhou 310027, China)

(<sup>2</sup>College of Engineering, Shantou University, Shantou 515063, China)

<sup>†</sup>E-mail: zju\_pxb@163.com

Received Oct. 9, 2016; Revision accepted Nov. 10, 2016; Crosschecked Oct. 29, 2017

**Abstract:** For the primary mirror of a large-scale telescope, an electro-hydraulic position control system (EHPCS) is used in the primary mirror support system. The EHPCS helps the telescope improve imaging quality and requires a micron-level position control capability with a high convergence rate, high tracking accuracy, and stability over a wide mirror cell rotation region. In addition, the EHPCS parameters vary across different working conditions, thus rendering the system nonlinear. In this paper, we propose a robust closed-loop design for the position control system in a primary hydraulic support system. The control system is synthesized based on quantitative feedback theory. The parameter bounds are defined by system modeling and identified using the frequency response method. The proposed controller design achieves robust stability and a reference tracking performance by loop shaping in the frequency domain. Experiment results are included from the test rig for the primary mirror support system, showing the effectiveness of the proposed control design.

**Key words:** Large-scale reflecting telescope; Quantitative feedback theory; Electro-hydraulic position control system; Micron-level position control capability; System identification; Robust stability

<https://doi.org/10.1631/FITEE.1601104>

**CLC number:** TH137; TP13

## 1 Introduction


A large-scale reflecting telescope (LSRT) is technology-intensive and a type of equipment used in many fields such as national security, space detection, and universe exploration (Bigongiari *et al.*, 2004; Jin *et al.*, 2013). These telescopes are equipped with large-diameter primary mirrors, to guarantee a strong light gathering power and high resolution. These superior abilities enable the LSRTs to explore

galaxies instantly from hundreds of millions of light years away. It is well understood that the primary mirror support system (PMSS) is a crucial component of the LSRT (Knohl, 1994; Stepp *et al.*, 1994). The PMSS bears the primary mirror weight and controls the mirror attitude toward the telescope mirror cell, without causing excessive surface deformation on the primary mirror. The telescope mirror cell rotates under various working conditions and the gravity distribution changes accordingly. Thereby, the external load on the PMSS changes. Consequently, the primary mirror can deviate from its original position for several or dozens of microns. For an LSRT, the doubly increased deviation has a serious impact on the telescope imaging quality.

An electro-hydraulic position control system (EHPCS) is applied to compensate for the deviation in

<sup>‡</sup> Corresponding author

\* Project supported by the National Basic Research Program (973) of China (No. 2013CB035400), the National High-Tech R&D Program (863) of China (No. 2012AA041803), and the National Natural Science Foundation of China (No. 51221004)

 ORCID: Xiong-bin PENG, <http://orcid.org/0000-0002-8120-4990>

© Zhejiang University and Springer-Verlag GmbH Germany 2017

the LSRT, thereby improving the telescope imaging quality. The EHPCS requires a micron-level position control capability from the controller along with high convergence rate, high tracking accuracy, and stability over a wide region.

The controller for EHPCS design problem, however, is challenging, in that the hydraulic part of the physical model is nonlinear. The system parameters vary under different working conditions, especially those related to temperature and pressure. Hydraulic fluid properties such as viscosity and bulk modulus show large uncertainties under different situations (Sirouspour and Salcudean, 2001), and as such contribute to the system nonlinearities. The system model also contains other types of nonlinearities, such as volume variations in the working chambers. Therefore, in this study we design a controller to overcome the nonlinearities and uncertainties in the EHPCS.

Two design methodologies are commonly used to deal with uncertainties in electro-hydraulic systems: adaptive control and robust control. Adaptive control typically identifies the plant parameters and system information online, and uses this information to tune the controller. The adaptive controller reduces the noise sensitivity and heavy memory requirements, while having a high accuracy in the tracking performance (Yao *et al.*, 2015). Robust control uses a fixed controller design and takes the worst case of uncertainties into consideration, to guarantee a system with better transient tracking performance and tracking accuracy regardless of time-varying uncertainties (Yao *et al.*, 2014).

In the EHPCS, a fixed controller is preferable for its feasibility. Several relevant robust techniques have been used in electro-hydraulic systems for years. Back-stepping (Yao *et al.*, 2014), H-infinity (Singh *et al.*, 2013), and model-predictive controllers (Bender *et al.*, 2015) are popular choices for position control systems. Yet, these methods face problems including limited accessibility for online calibration or heavy computational loads. Moreover, the controllers are of high order and face great difficulties during the implementation.

Given these challenges, we present a new method based on quantitative feedback theory (QFT) to deal with the uncertainties in an EHPCS. The QFT technique is an efficient and robust control design

method, which has been successfully implemented in many kinds of systems, such as single input and single output (SISO) systems, multiple input and single output (MISO) systems, multiple input and multiple output (MIMO) systems, non-minimum phase systems, and unstable systems (Chait and Yaniv, 1993; Safarzadeh *et al.*, 2011; Wang *et al.*, 2011; Khodabakhshian and Hemmati, 2012; Moeinkhah *et al.*, 2014; Park *et al.*, 2014). This technique provides systems with stability and robust reference tracking ability, yet it can be applied as easily as proportional-integral-derivative (PID) controllers. The QFT controller design for the EHPCS is divided into three steps: (1) EHPCS system modeling, (2) parameter identification for different working conditions, and (3) controller design with the desired stability margins. A set of linearized models is the base for the QFT controller design. To demonstrate the robust capability of the controller design, experiments are carried out to examine the transient tracking performance under different working conditions.

## 2 System description

### 2.1 Basic structure

Fig. 1 shows the schematic of the EHPCS, which includes a DC motor, a screw, an amplifying cylinder with a small effective area, a supporting cylinder with a large effective area, an accumulator, and two transmission pipes.

In this system, the primary mirror attitude toward the mirror cell is determined by the displacement of the supporting cylinders in several EHPCSs. In applications using the reflecting telescope technique, both the dynamic response and positioning accuracy are important for high imaging quality. Thus, a large effective area ratio between the supporting cylinder and the amplifying cylinder is chosen to assure the micron-level positioning accuracy, and a DC motor is used to guarantee a fast dynamic response. The screw converts the DC motor rotation into the amplifying cylinder translation, thereby determining the flow direction between two working chambers (whose volumes are  $V_1$  and  $V_2$ , respectively). The accumulator provides the EHPCS with a steady working pressure. Since the volume changes

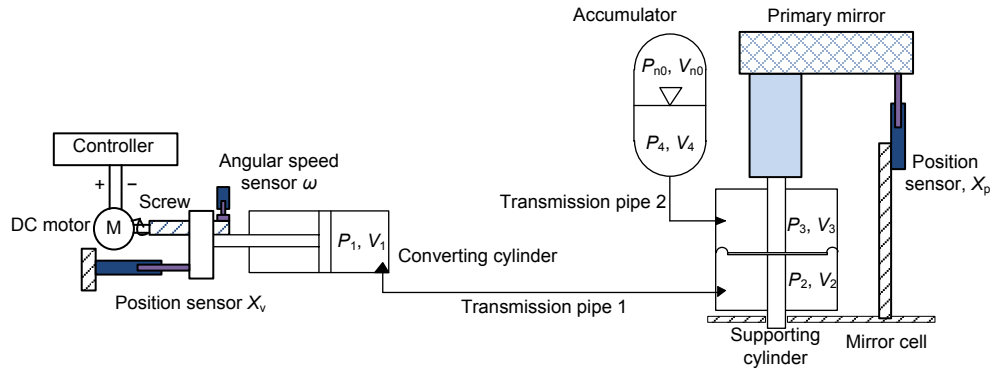


Fig. 1 Schematic of the electro-hydraulic position control system (EHPCS) for a large-scale reflecting telescope

are very small compared to the accumulator pre-charged volume, the accumulator pressure hardly changes.

The following sensors are installed in the system to monitor the hardware configurations:

1. a pressure sensor measuring the pressure  $P_2$  in the lower chamber of the supporting cylinder;
2. a pressure sensor measuring the pressure  $P_3$  in the upper chamber of the supporting cylinder;
3. an angular speed sensor measuring the angular speed  $\omega$  of the DC motor;
4. a magneto telescopic position sensor measuring the position  $X_v$  of the amplifying cylinder;
5. a linear variable differential transformer (LVDT) position sensor measuring the position  $X_p$  of the supporting cylinder;
6. the temperature sensor measuring the temperature  $T$  of the supporting cylinder.

The SISO position control system based on this hardware configuration is depicted in Fig. 2. In this system, the supporting cylinder displacement  $X_p$  is the control target. The desired position is predesigned and compared to the position feedback signal. Through the controller action, the DC motor produces a reasonable rotation and then determines the motion of the amplifying cylinder, and thereby changes the supporting cylinder displacement through the transmission of hydraulic fluid.

## 2.2 System modeling of EHPCS

Based on the hardware configuration (Fig. 1) and control schematic diagram (Fig. 2), the EHPCS can be divided into three parts: (1) the electric part from the controller output voltage  $U_0$  to the DC motor output angular speed, (2) the mechanical transmission part from the DC motor output angular speed to the amplifying cylinder displacement, and (3) the hydraulic fluid transmission from the amplifying cylinder displacement to the supporting cylinder displacement.

First, the speed controller is well designed so that the transfer function of the electric part is strictly a first-order system:

$$P_1(s) = \frac{\omega(s)}{U_0(s)} = \frac{K_{uv}}{T_{uv}s + 1}, \quad (1)$$

where  $K_{uv}$  is the steady-state gain and  $T_{uv}$  the time constant. The speed controller design will not be expanded in this study.

Second, according to the working principle of the mechanical screw, which is considered to be a rigid transmission, the transfer function of the mechanical part is shown as

$$P_2(s) = \frac{X_v(s)}{\omega(s)} = \frac{l_s}{2\pi s}, \quad (2)$$

where  $l_s$  is the screw pitch.

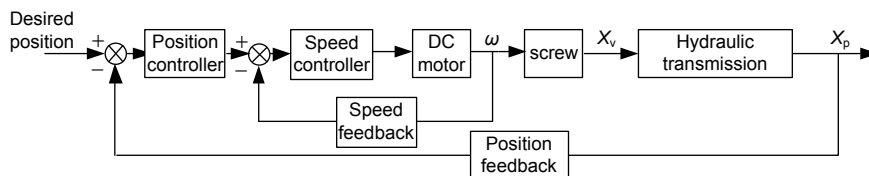


Fig. 2 Schematic of the electro-hydraulic position control system (EHPCS)

Third, assume that the hydraulic fluid bulk modulus and viscosity are constants. Applying the law of continuity to each working chamber, the load-flow continuity equations for the hydraulic transmission part are given as

$$\frac{dV_1}{dt} + \frac{V_1}{E_h} \frac{dP_1}{dt} = -Q_1 - k_{c1}P_1, \quad (3)$$

$$\frac{dV_2}{dt} + \frac{V_2}{E_h} \frac{dP_2}{dt} = Q_2 - k_{c2}P_2, \quad (4)$$

$$\frac{dV_3}{dt} + \frac{V_3}{E_h} \frac{dP_3}{dt} = -Q_3 - k_{c3}P_3, \quad (5)$$

$$\frac{dV_4}{dt} + \frac{V_4}{E_h} \frac{dP_4}{dt} = Q_4 - k_{c4}P_4, \quad (6)$$

where  $E_h$  is the oil bulk modulus,  $k_{c1}$ ,  $k_{c2}$ ,  $k_{c3}$ ,  $k_{c4}$  the leakage coefficients of each working chamber, and  $Q_1$ – $Q_4$  the flow volume of the corresponding working chamber.

For simplification, the effects of the transmission pipes are neglected, which gives the following expressions:

$$P_1 = P_2, P_3 = P_4, Q_1 = Q_2, Q_3 = Q_4. \quad (7)$$

According to Eq. (7) and ignoring fluid leakage, Eqs. (3)–(6) can be simplified as

$$-A_v \dot{X}_v + \frac{V_{01} - A_v X_v}{E_h} \frac{dP_1}{dt} = -Q_1, \quad (8)$$

$$A_p \dot{X}_p + \frac{V_{02} + A_p X_p}{E_h} \frac{dP_1}{dt} = Q_1, \quad (9)$$

$$-A_p \dot{X}_p + \frac{V_{03} - A_p X_p}{E_h} \frac{dP_3}{dt} = -Q_3, \quad (10)$$

$$\frac{dV_4}{dt} + \frac{V_4}{E_h} \frac{dP_4}{dt} = Q_4, \quad (11)$$

where  $A_v$  is the pressure area of the amplifying cylinder,  $A_p$  the pressure area of the supporting cylinder, and  $V_{01}$ ,  $V_{02}$ , and  $V_{03}$  the initial volumes of the corresponding working chambers. Combining Eqs. (8) and (9), we obtain

$$A_p \dot{X}_p - A_v \dot{X}_v = \frac{A_v X_v - A_p X_p - (V_{01} + V_{02})}{E_h} \frac{dP_2}{dt}. \quad (12)$$

The state equation for nitrogen in the accumulator can be described as

$$\begin{aligned} P_{n0} V_{n0} &= (P_{n0} + dP_4)(V_{n0} + dV_n) \\ &= P_{n0} V_{n0} + V_{n0} dP_4 + P_{n0} dV_n + dP_4 dV_n, \end{aligned} \quad (13)$$

where  $P_{n0}$  and  $V_{n0}$  are the initial pressure and volume of nitrogen in the accumulator, respectively. Note that

$$dV_n + dV_4 = 0. \quad (14)$$

Then according to Eq. (13), we obtain

$$\frac{dV_4}{dt} \approx \frac{V_{n0}}{P_{n0}} \frac{dP_4}{dt}. \quad (15)$$

Combining Eqs (10), (11), and (15), we obtain

$$A_p \dot{X}_p = \left( \frac{V_{n0}}{P_{n0}} + \frac{V_4 + V_{03} - A_p X_p}{E_h} \right) \frac{dP_3}{dt}. \quad (16)$$

Note that the system works at a low pressure ranging from  $2 \times 10^5$  to  $5 \times 10^5$  Pa. Thus, we can easily obtain

$$\frac{V_{n0}}{P_{n0}} \gg \frac{V_4 + V_{03} - A_p X_p}{E_h}. \quad (17)$$

Then Eq. (16) can be simplified as

$$A_p \dot{X}_p = \frac{V_{n0}}{P_{n0}} \frac{dP_3}{dt}. \quad (18)$$

By applying Newton's second law, the supporting cylinder's force balance equation is

$$m_2 \ddot{X}_p + B_p \dot{X}_p = A_p (P_2 - P_3) - G - F_L. \quad (19)$$

where  $m_2$ ,  $F_L$ ,  $G$ , and  $B_p$  are the equivalent mass, the external load, the gravity, and the equivalent damping ratio of the supporting cylinder, respectively.

Combining Eqs. (12), (16), and (19), and proceeding with a Laplace transform, we can obtain

$$\begin{aligned} A_p X_p - A_v X_v &= \frac{A_v X_v - A_p X_p - (V_{01} + V_{02})}{E_h} P_2 \\ &\approx -\frac{V_{01} + V_{02}}{E_h} P_2, \end{aligned} \quad (20)$$

$$A_p X_p = \frac{V_{n0}}{P_{n0}} P_3, \quad (21)$$

$$m_2 s^2 X_p + B_p s X_p = A_p (P_2 - P_3) - G - F_L. \quad (22)$$

From Eqs. (20)–(22), the transfer function from the amplifying cylinder displacement to the supporting cylinder displacement can be depicted as

$$P_3(s) = \frac{X_p(s)}{X_v(s)} = \frac{A_v / A_p}{1 + \frac{V_0 m_2 s^2}{A_p^2 E_h} + \frac{V_0 B_p s}{A_p^2 E_h} + \frac{V_0 P_{n0}}{V_{n0} E_h}}. \quad (23)$$

Note that all the three parts contribute to the entire EHPCS. The overall plant can be expressed as

$$P(s) = P_1(s) \cdot P_2(s) \cdot P_3(s). \quad (24)$$

According to Eqs. (1), (2), (23), and (24), the abovementioned linear EHPCS system is a serial combination of a first-order system, an integrator, and a second-order system, based on several assumptions. However, due to the system uncertainties caused by the changes in the working environment, the position controller may face the risk of being unstable or losing its tracking ability. Taking the system nonlinearities into consideration, the position controller design must preserve a robust margin for each critical working condition. This design robustness plays an important role when facing parameter uncertainties in the EHPCS, including the change of fluid bulk modulus, viscosity, accumulator pressure at different temperatures, and the working chamber volumes during the position tracking procedure.

In summary, this study aims to present a robust controller design algorithm for the EHPCS in an LSRT primary mirror support system, such that the supporting system displays superior behavior regardless of the changes in working conditions. In addition, the proposed controller should be feasible for implementation into the auto-control system.

### 3 System parameter identification for EHPCS

When the environmental temperature changes, the system variables (e.g., fluid bulk modulus, vis-

cosity, and accumulator pressure) face uncertainty. Therefore, the next step in designing a robust controller is to identify a set of EHPCS parameters, especially for the hydraulic fluid transmission part, under different working conditions. These working conditions should cover the whole working environment that the EHPCS will encounter. Sweep sine wave signals (SSWSs) are selected as persistent excitation to the plant, because they can cover the working frequency range of the EHPCS. Given the particular application of the LSRT, the rising time of a 20- $\mu\text{m}$  step response is restricted to be smaller than 200 ms, which means that the natural frequency of the position control system is about 9 rad/s (or  $9/(2\pi)$  Hz), according to Eq. (25):

$$t_r \approx \frac{1.8}{\omega_n}. \quad (25)$$

Consequently, the SSWS frequency ranges from 0.1 to 20 Hz (20 Hz is five times more than the system's natural frequency).

#### 3.1 Identification setup

In this study, we focus on the uncertainties of EHPCS parameters, which are caused mainly by hydraulic nonlinearities. Thus, when we identify the system information, only the hydraulic fluid transmission part is considered. The amplifying cylinder displacement is chosen as the input signal and the supporting cylinder displacement as the output signal. For this particular application, an underdamped second-order system model is preferred, and the corresponding transfer function is shown as

$$P'_3(s) = \frac{K}{As^2 + Bs + 1}. \quad (26)$$

Our goal is to determine a set of parameters  $\{[A_1, B_1, K_1], [A_2, B_2, K_2], \dots, [A_n, B_n, K_n]\}$  under typical working conditions. The excitation experiments are carried out at different environmental temperatures: 25, 10, and  $-5^\circ\text{C}$ . In addition, the experiments are carried out at different initial positions of the amplifying cylinder: left position, middle position, and right position. Accordingly, nine cases, denoted by case 1 to case 9, are investigated to generate the linear plant's family.

The position signals are detected by position sensors, and the sampling time interval is 1 ms. The

experiment data is then exported to the MATLAB identification toolbox. The sampled data for each case is divided into two subparts, one for the identification of parameters by using the frequency response method and the other for model validation. Figs. 3a and 3b show the displacement signal samples for identification in case 1, where the environmental temperature is 25 °C and the amplifying cylinder is at the left initial position. The identified model for case 1 is shown in Fig. 3c. A percentage index, defined as a normalized L2-norm of the residual signal between the measured output and the simulated output, is used to determine the modeling accuracy. In case 1, the accuracy index is as high as 89%, which means that the simulated model behaves rather similarly to the actual system.

### 3.2 Identification results

The identification results from case 1 through case 9 are listed in Table 1. For all the cases, the accuracy indices are higher than 85%, which means that the hydraulic fluid transmission part can be well represented by a second-order transfer function, and that the modeling description in Section 2 is reliable. The identified parameters vary apparently between different cases. When the environmental temperature rises, the system's natural frequency increases, and the damping ratio jumps. Compared with the environmental temperature influence, the initial position of the amplifying cylinder has less influence on the parameter values.

To summarize, the overall open-loop transfer function of the EHPCS from controller voltage to supporting cylinder displacement can be described as Eq. (27), and the lower and upper bounds of system parameters are as listed in Table 2.

$$P(s) = \frac{K_{uv}}{T_{uv}s + 1} \frac{l_s}{2\pi s} \frac{1}{As^2 + Bs + 1} \frac{K}{As^2 + Bs + 1} \quad (27)$$

$$= K_{uvl} \frac{1}{T_{uv}s + 1} \frac{1}{s} \frac{K}{As^2 + Bs + 1}$$

## 4 QFT controller design

As confirmed in Section 3, the EHPCS parameters are largely uncertain, and therefore a robust control design method, namely quantitative feedback

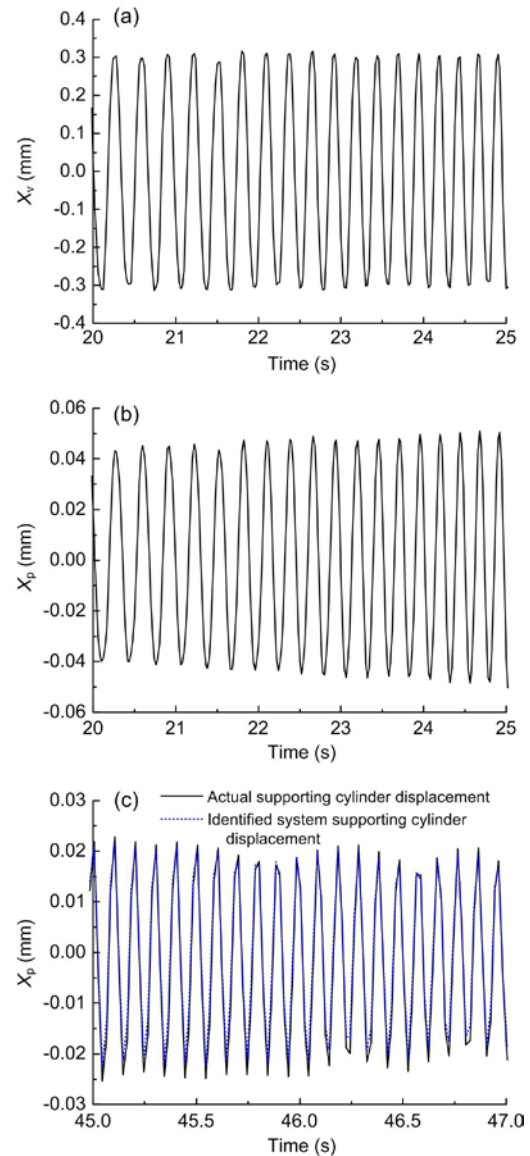


**Fig. 3** Sine wave sweep excitation displacement signal fragment for the amplifying cylinder (a), measured output displacement signal fragment for the supporting cylinder (b), and model validation for the identified system (c)

theory (QFT), is proposed in this section. The aim of this method is to achieve the desired closed-loop performance in the face of model uncertainties and disturbances.

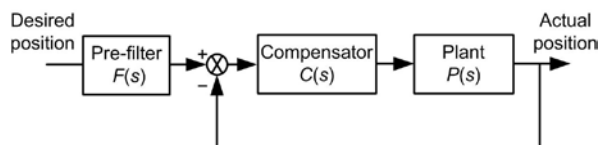
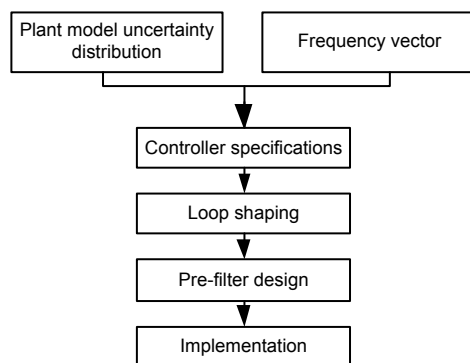
The QFT controller is a two-degree-of-freedom feedback controller (Fig. 4). There are five steps (Fig. 5) to well design the compensator  $C(s)$  and pre-filter  $F(s)$  to achieve the desired robust stability and performance specifications.

**Table 1 Parameter identification results under different working conditions**

Case index	$\zeta$	$\omega_n$ (rad/s)	$A$ ((rad/s) <sup>-2</sup> )	$B$ ((rad/s) <sup>-1</sup> )	$K$	$T$ (°C)	$P_3$ ( $\times 10^5$ Pa)	Position	Accuracy
1	0.3033	46.5	$4.62 \times 10^{-4}$	0.01305	0.1173	25	3.50	Left	89.3%
2	0.2932	49.3	$4.11 \times 10^{-4}$	0.01189	0.1072	25	3.63	Middle	86.8%
3	0.2841	56.3	$3.15 \times 10^{-4}$	0.01009	0.1132	25	3.75	Right	90.3%
4	0.4102	43.5	$5.28 \times 10^{-4}$	0.01885	0.1232	10	3.23	Left	85.3%
5	0.4056	44.3	$5.09 \times 10^{-4}$	0.01831	0.1135	10	3.35	Middle	87.6%
6	0.3817	45.9	$4.75 \times 10^{-4}$	0.01663	0.1203	10	3.45	Right	89.1%
7	0.5912	40.4	$6.13 \times 10^{-4}$	0.02967	0.1132	-5	3.03	Left	90.5%
8	0.5867	41.2	$5.89 \times 10^{-4}$	0.02848	0.1096	-5	3.08	Middle	86.3%
9	0.5812	41.7	$5.75 \times 10^{-4}$	0.02787	0.1024	-5	3.16	Right	87.4%

**Table 2 Parameter bounds for the linear plant family**

Parameter	Unit	Upper bound	Lower bound
$K_{uv1}$	$\mu\text{m}/(\text{s} \cdot \text{V})$	6667	6667
$T_{uv1}$	s	0.002	0.002
$A$	(rad/s) <sup>-2</sup>	$5.75 \times 10^{-4}$	$4.62 \times 10^{-4}$
$B$	(rad/s) <sup>-1</sup>	0.02787	0.01305
$K$	—	0.1232	0.1024

**Fig. 4 Quantitative feedback theory (QFT) control system feedback structure****Fig. 5 The quantitative feedback theory (QFT) design framework**

In the first step, distributions of the parameter uncertainties and nominal parameters are specified. Additionally, plant frequencies should be defined overall for the stages in the design. Then, a template for each plant frequency is generated, representing the frequency response of the plant including the

uncertainties, in the Nichols chart. After the template generation process, desired controller specifications such as robust stability, disturbance rejection, and robust reference tracking are defined. Concurrently, the controller specifications are calculated and visualized in the Nichols chart in the second step. The compensator is designed in the third step, based on the open-loop frequency-response analysis of the nominal plant. In the fourth step, a pre-filter is designed to achieve the intended reference tracking robustness.

#### 4.1 Template generation

The discrete frequency vector represents an important criterion during the design process. The templates are generated for the EHPCS at seven chosen frequencies. For this particular application, the most important frequency mentioned in Section 3 is  $9/(2\pi)$  Hz, so the frequency vector of this closed-loop control is chosen as follows:

$$\begin{aligned}\omega &= 2\pi[f_1, f_2, f_3, f_4, f_5, f_6, f_7] \\ &= 2\pi[0.1, 0.5, 1, 2, 5, 10, 50].\end{aligned}\quad (28)$$

The EHPCS model is described as a transfer function shown in Eq. (27) with parameter uncertainties, and the parameter bounds are summarized in Section 3 and listed in Table 2.

#### 4.2 Performance specifications

After the template generation process, two performance specifications are proposed: robust stability and robust reference tracking ability.

##### 1. Robust stability

This specification is represented by the peak response ( $M_p$ ):

$$\left| \frac{C(s)P(s)}{1 + C(s)P(s)} \right| \leq M_p, \quad \forall \omega \in [0, \infty), \quad (29)$$

where  $C(s)$  is the compensator transfer function, and  $P(s)$  is the plant transfer function with uncertainties. As a reliable stability criterion, the peak response reflects the control quality in the time domain such as overshoot. Practically speaking, the phase margin should be about  $55^\circ$ , which gives  $M_p$  a value of 1.1, according to the maximum peak criterion:

$$\begin{cases} \text{GM} = 20 \log \left( 1 + \frac{1}{M_p} \right), \\ \text{PM} = 2 \arcsin \left( \frac{1}{2M_p} \right), \end{cases} \quad (30)$$

where GM and PM are gain and phase margins, respectively.

## 2. Robust reference tracking ability

This specification determines the lower and upper tracking bounds of the closed-loop system control ratio, which can be expressed as follows:

$$|T_L(j\omega)| \leq \left| \frac{F(s)C(s)P(s)}{1 + C(s)P(s)} \right| \leq |T_U(j\omega)|, \quad \forall \omega \in [0, \infty), \quad (31)$$

where  $F(s)$  is the pre-filter transfer function, and  $T_L$  and  $T_U$  are the lower and upper tracking bounds, respectively.

In this particular application,  $T_L$  should promise a closed-loop step response with a settling time of 0.4 s and no overshoot, and  $T_U$  should guarantee the step response with a rising time of 60 ms and 10% overshoot. Using the MATLAB SISO design toolbox, the lower and upper bounds are respectively chosen as

$$T_L(j\omega) = \frac{1}{\left( \frac{s}{15} + 1 \right) \left( \frac{s}{20} + 1 \right) \left( \frac{s}{190} + 1 \right) \left( \frac{s}{190} + 1 \right)}, \quad (32)$$

$$T_U(j\omega) = \frac{\left( \frac{s}{10} + 1 \right) \left( \frac{s}{120} + 1 \right)}{\left( \frac{s}{17} + 1 \right) \left( \frac{s}{30} + 1 \right) \left( \frac{s}{30} + 1 \right)}. \quad (33)$$

## 4.3 Loop-shaping

After the definition of the specifications, the composite bounds would be specified in the Nichols chart (Fig. 6), which is used to synthesize the open-loop transfer function. The composite bounds contain the worst case for the controller design.

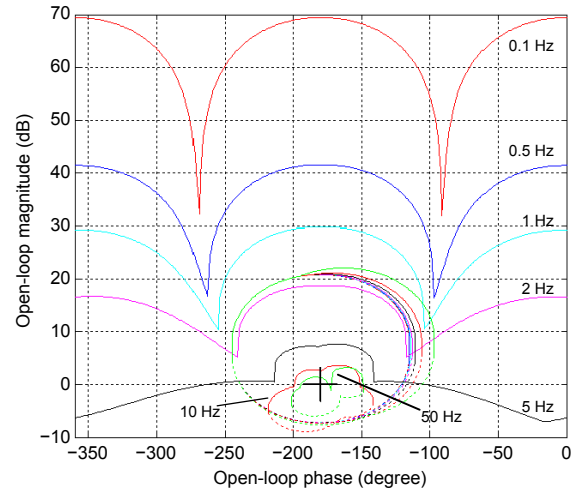


**Fig. 6 The quantitative feedback theory (QFT) composite bounds in the Nichols chart**

By adding reasonable poles and zeroes, the nominal transfer function is shaped to satisfy the composite bounds at the chosen frequencies. Thus, the closed-loop system can behave within all specification bounds. Some guidelines have been provided to shape the nominal transfer function. The most important one is that the shaped transfer function should fulfill the bounds and decrease as rapidly as possible with the frequency to keep the controller bandwidth small (Chatlatanagulchai *et al.*, 2016). An appropriate compensator design is shown in Fig. 7, which is accomplished allowing for a trade-off between controller complexity and performance specifications. The compensator containing two real poles and two real zeroes is illustrated as

$$C(s) = \frac{0.017 \left( \frac{s}{100} + 1 \right) \left( \frac{s}{363} + 1 \right)}{\left( \frac{s}{30} + 1 \right) \left( \frac{s}{300} + 1 \right)}. \quad (34)$$

The compensator in Eq. (34) fulfills the composite bounds and guarantees the nominal closed-loop



system step response with a rising time of 0.05 s, an overshoot of 1.37%, and a settling time of 0.21 s.

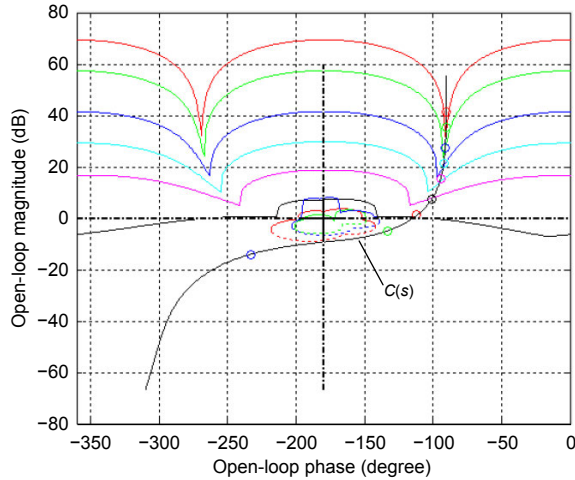


Fig. 7 The quantitative feedback theory (QFT) loop-shaping results in the Nichols chart

#### 4.4 Pre-filter design

After the loop-shaping process, the next step is to design the pre-filter. The pre-filter helps in that the magnitude of the close-loop frequency response lies within the lower and upper reference tracking bounds. For this particular application, a real zero, a pair of complex zeroes, and a real pole are added to the pre-filter. Taking the physical feasibility into consideration, two large supplementary real poles are added to the pre-filter. Then the pre-filter design result is shown as

$$F(s) = \frac{\left(\frac{s}{87.67} + 1\right) \left(\left(\frac{s}{37.6}\right)^2 + \frac{1.04s}{37.6} + 1\right)}{\left(\frac{s}{32.47} + 1\right) \left(\frac{s}{222.9} + 1\right) \left(\frac{s}{290} + 1\right)}. \quad (35)$$

The corresponding tracking bounds of Eq. (35) are presented in Fig. 8. Although the maximum and minimum closed-loop frequency responses do not exactly lie within the predesigned upper and lower bound model, the design result is acceptable.

## 5 Controller implementation and validation

In this section, the performance of QFT controller design is validated on a primary mirror support

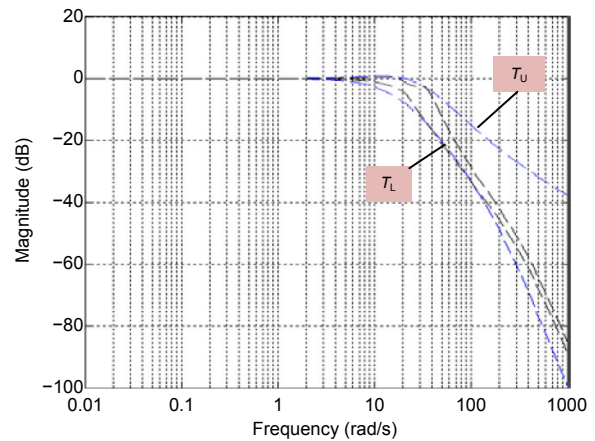


Fig. 8 The quantitative feedback theory (QFT) pre-filter design results displayed as a Bode plot

test rig. The EHPCS is applied to compensate for the deviation in the primary mirror support system (Fig. 9). Thus, the step closed-loop response performance under various working environments is the most crucial property. A typical set of performance requirements is listed as follows:

1. rising time  $t_r$ : less than 200 ms;
2. overshoot  $M_p$ : less than 20%;
3. settling time  $t_s$ : less than 400 ms;
4. steady state error  $e_{ss}$ : less than 0.5  $\mu\text{m}$ .

Knowing that the system suffers from larger uncertainties under changed temperatures than from other variables, the EHPCS closed-loop performance is evaluated at typical working temperatures of  $-5$ ,  $10$ , and  $25$   $^{\circ}\text{C}$ . For this validation experiment, the QFT controller closed-loop 20- $\mu\text{m}$  step response is compared with that of a well-tuned PID controller, which is widely used in the field of electro-hydraulic position control (Liu and Daley, 1999; Ahn *et al.*, 2007; Elbayomy *et al.*, 2008). All the experiments were performed on the experiment rig (Fig. 9).

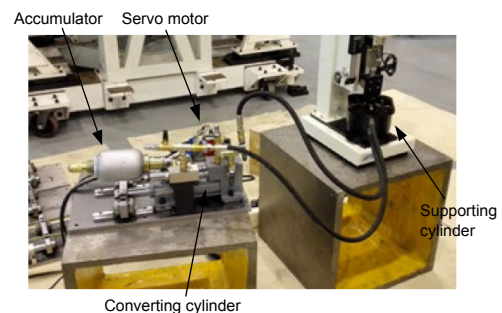
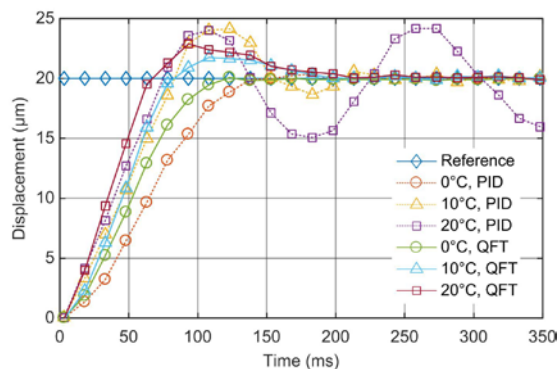


Fig. 9 The electro-hydraulic position control system (EHPCS) experiment rig

For the first attempt, a PID controller was well tuned at a working temperature of  $-5^{\circ}\text{C}$ , and then the PID controller performance was evaluated at the two other temperatures. For the second attempt, the QFT controller including a compensator and a pre-filter, as described in Section 4, was implemented to examine the closed-loop robust stability of the step response in the time domain at all three working temperatures.

Fig. 10 shows the test results for the PID controller and the QFT controller. Clearly, the EHPCS at a working temperature of  $-5^{\circ}\text{C}$  performs with a satisfactory closed-loop step response with a rising time of 130 ms, a slight overshoot of 1.75%, and a settling time of 150 ms. As the temperature goes up to  $10^{\circ}\text{C}$ , the closed-loop step response becomes less satisfactory. Although the rising time is less than 100 ms, the overshoot increases substantially to 20.7%. Moreover, the settling time under such conditions is about 250 ms. When the EHPCS works at  $25^{\circ}\text{C}$ , oscillations occur in the closed-loop system step response, which makes the PID controller unacceptable. Since the EHPCS working conditions vary largely, the PID controller seems to be impractical for the EHPCS.



**Fig. 10** The electro-hydraulic position control system (EHPCS) closed-loop step responses of PID and QFT controllers under different temperatures

PID: proportional-integral-derivative; QFT: quantitative feedback theory

Similar to the PID controller, the EHPCS at a low temperature of  $-5^{\circ}\text{C}$  performs with a superior closed-loop step response with a rising time of 100 ms, a settling time of 120 ms, and no overshoot. As the temperature climbs, the overshoot becomes greater, and the settling time becomes longer. No oscillation is observed at the relatively high temperature. It can be seen from Fig. 10 that the EHPCS with the QFT

controller satisfies the performance requirements regardless of changes to the working temperature.

To summarize, the PID controller ensures that the EHPCS operates with acceptable specifications at certain temperatures, yet it becomes impractical when the EHPCS suffers from large environmental temperature changes. The QFT controller can survive under extreme environmental temperature changes and perform with a stable behavior.

## 6 Conclusions

A robust controller design for the EHPCS in an LSRT primary mirror support system has been presented in this paper. The design method is based on quantitative feedback theory. The plant is modeled and its parameters are identified from different working conditions such as environmental temperature and the initial working position. The plant identification results indicated that the modeling procedure is reliable and could thus determine the uncertainty bounds for the parameters. Using the quantitative feedback theory (QFT) design framework, the robust control loop for EHPCS was designed taking into consideration the parameter uncertainties and controller specifications. Validation experiments including the proposed controller and a well-tuned PID controller were carried out under different working temperatures of an EHPCS. The results showed that the proposed controller presents superior performance with a more robust stability compared with the PID controller. This EHPCS control design methodology has value for LSRTs operating in extreme conditions and especially for LSRTs located in relatively high latitude areas.

## References

- Ahn, K.K., Truong, D.Q., Soo, Y.H., 2007. Self tuning fuzzy PID control for hydraulic load simulator. 6th Int. Conf. on Control, Automation, and Systems, p.345-349. <https://doi.org/10.1109/ICCAS.2007.4406935>
- Bender, F.A., Sonntag, M., Sawodny, O., 2015. Nonlinear model predictive control of a hydraulic excavator using Hammerstein models. 6th Int. Conf. on Automation, Robotics and Applications, p.557-562. <https://doi.org/10.1109/ICARA.2015.7081208>
- Bigongiari, C., Bastieri, D., Galante, N., et al., 2004. The MAGIC telescope reflecting surface. *Nucl. Instr. Meth. Phys. Res. A*, **518**(1-2):193-194. <https://doi.org/10.1016/j.nima.2003.10.058>

- Chait, Y., Yaniv, O., 1993. Multi-input/single-output computer-aided control design using the quantitative feedback theory. *Int. J. Robust Nonl. Contr.*, **3**(1):47-54. <https://doi.org/10.1002/rnc.4590030103>
- Chatlatanagulchai, W., Kijdech, D., Benjalersyarnon, T., et al., 2016. Quantitative feedback input shaping for flexible-joint robot manipulator. *J. Dynam. Syst. Meas. Contr.*, **138**(6):061006. <https://doi.org/10.1115/1.4032931>
- Elbayomy, K.M., Jiao, Z.X., Zhang, H.Q., 2008. PID controller optimization by GA and its performances on the electro-hydraulic servo control system. *Chin. J. Aeronaut.*, **21**(4):378-384. [https://doi.org/10.1016/S1000-9361\(08\)60049-7](https://doi.org/10.1016/S1000-9361(08)60049-7)
- Jin, H., Lim, J., Kim, Y., et al., 2013. Optical design of a reflecting telescope for CubeSat. *J. Opt. Soc. Korea*, **17**(6):533-537. <https://doi.org/10.3807/JOSK.2013.17.6.533>
- Khodabakhshian, A., Hemmati, R., 2012. Robust decentralized multi-machine power system stabilizer design using quantitative feedback theory. *Int. J. Electr. Power Energy Syst.*, **41**(1):112-119. <https://doi.org/10.1016/j.ijepes.2012.03.023>
- Knohl, E.D., 1994. VLT primary support system. SPIE, **2199**:271-283. <https://doi.org/10.1117/12.176196>
- Liu, G.P., Daley, S., 1999. Optimal-tuning PID controller design in the frequency domain with application to a rotary hydraulic system. *Contr. Eng. Pract.*, **7**(7):821-830. [https://doi.org/10.1016/S0967-0661\(99\)00047-7](https://doi.org/10.1016/S0967-0661(99)00047-7)
- Moeinkhah, H., Akbarzadeh, A., Rezaeepazhand, J., 2014. Design of a robust quantitative feedback theory position controller for an ionic polymer metal composite actuator using an analytical dynamic model. *J. Intell. Mater. Syst. Struct.*, **25**(15):1965-1977. <https://doi.org/10.1177/1045389X13512906>
- Park, I., Hong, S., Sunwoo, M., 2014. Robust air-to-fuel ratio and boost pressure controller design for the EGR and VGT systems using quantitative feedback theory. *IEEE Trans. Contr. Syst. Technol.*, **22**(6):2218-2231. <https://doi.org/10.1109/TCST.2014.2301160>
- Safarzadeh, O., Khaki-Sedigh, A., Shirani, A.S., 2011. Identification and robust water level control of horizontal steam generators using quantitative feedback theory. *Energy Conv. Manag.*, **52**(10):3103-3111. <https://doi.org/10.1016/j.enconman.2011.04.023>
- Singh, V.P., Mohanty, S.R., Kishor, N., et al., 2013. Robust H-infinity load frequency control in hybrid distributed generation system. *Int. J. Electr. Power Energy Syst.*, **46**:294-305. <https://doi.org/10.1016/j.ijepes.2012.10.015>
- Sirouspour, M.R., Salcudean, S.E., 2001. Nonlinear control of hydraulic robots. *IEEE Trans. Robot. Autom.*, **17**(2):173-182. <https://doi.org/10.1109/70.928562>
- Stepp, L.M., Huang, E., Cho, M.K., 1994. Gemini primary mirror support system. SPIE, **2199**:223-238. <https://doi.org/10.1117/12.176192>
- Wang, Y.Y., Haskara, I., Yaniv, O., 2011. Quantitative feedback design of air and boost pressure control system for turbocharged diesel engines. *Contr. Eng. Pract.*, **19**(6):626-637. <https://doi.org/10.1016/j.conengprac.2011.02.006>
- Yao, J.Y., Jiao, Z.X., Ma, D.W., 2014. Extended-state-observer-based output feedback nonlinear robust control of hydraulic systems with backstepping. *IEEE Trans. Ind. Electron.*, **61**(11):6285-6293. <https://doi.org/10.1109/TIE.2014.2304912>
- Yao, J.Y., Jiao, Z.X., Ma, D.W., 2015. A practical nonlinear adaptive control of hydraulic servomechanisms with periodic-like disturbances. *IEEE/ASME Trans. Mechatron.*, **20**(6):2752-2760. <https://doi.org/10.1109/TMECH.2015.2409893>